Analysis of heat flow in layered structures for time-domain thermoreflectance

Cite as: Review of Scientific Instruments **75**, 5119 (2004); https://doi.org/10.1063/1.1819431
Submitted: 11 June 2004 . Accepted: 19 September 2004 . Published Online: 10 November 2004

David G. Cahill

Analysis of heat flow in layered structures for time-domain thermoreflectance

David G. Cahill[a)]
Department of Materials Science and Engineering and Frederick Seitz Materials Research Laboratory, University of Illinois, Urbana, Illinois 61801

(Received 11 June 2004; accepted 19 September 2004; published 10 November 2004)

The iterative algorithm of Feldman for heat flow in layered structures is solved in cylindrical coordinates for surface heating and temperature measurement by Gaussian-shaped laser beams. This solution for the frequency-domain temperature response is then used to model the lock-in amplifier signals acquired in time-domain thermoreflectance measurements of thermal properties. © *2004 American Institute of Physics.* [DOI: 10.1063/1.1819431]

I. INTRODUCTION

Time-domain thermoreflectance (TDTR) is a pump-probe optical technique that can be used for measuring the thermal properties of materials.[1–5] We have previously described our implementation of this technique,[6,7] and our application of this method in studies of the thermal conductivity of thin films,[8,9] the thermal conductance of interfaces,[8,10] spatially resolved measurements of microfabricated structures,[10] and high-resolution mapping of the thermal conductivity of diffusion multiples.[11]

In most cases, analysis of TDTR experiments requires comparisons between the data and a model of the heat transport in the system under study. Unknown thermal properties are treated as free parameters and adjusted to minimize the differences between the model and the data. We have briefly described how the frequency-domain thermal response can be used as the input to a calculation of the in-phase and out-of-phase lock-in amplifier signals in TDTR experiments[8,11] but we have not previously described our method for calculating the frequency-domain response. The purpose of this article is to describe the details of those calculations and provide additional discussion of our methods for analyzing TDTR data.

II. FREQUENCY DOMAIN SOLUTION FOR THE SURFACE TEMPERATURE OF A SINGLE LAYER

We begin with the frequency-domain solution[12] for a semi-infinite solid that is heated at the surface by a periodic point source of unit power at angular frequency ω

$$g(r) = \frac{\exp(-qr)}{2\pi\Lambda r}, \tag{1}$$

$$q^2 = (i\omega/D), \tag{2}$$

where Λ is the thermal conductivity of the solid, D the thermal diffusivity, and r the radial coordinate. This solution for the semi-infinite solid differs from the solution for the infinite solid by a factor of 2. Since the co-aligned laser beams of a typical TDTR experiment have cylindrical symmetry, we use Hankel transforms[13,14] to simplify the convolution of this solution with the distributions of the laser intensities. The Hankel transform of $g(r)$ is

$$G(k) = 2\pi \int_0^\infty g(r) J_0(2\pi k r)\, r\, dr, \tag{3}$$

$$G(k) = \frac{1}{\Lambda(4\pi^2 k^2 + q^2)^{1/2}}. \tag{4}$$

The surface is heated by a pump laser beam with a Gaussian distribution of intensity $p(r)$; the $1/e^2$ radius of the pump beam is w_0.

$$p(r) = \frac{2A}{\pi w_0^2} \exp(-2r^2/w_0^2), \tag{5}$$

where A is the amplitude of the heat absorbed by the sample at frequency ω. The Hankel transform of $p(r)$ is

$$P(k) = A \exp(-\pi^2 k^2 w_0^2/2). \tag{6}$$

The distribution of temperature oscillations at the surface $\theta(r)$ is the inverse transform of the product of $G(k)$ and $P(k)$

$$\theta(r) = 2\pi \int_0^\infty P(k) G(k) J_0(2\pi k r)\, k\, dk. \tag{7}$$

The surface temperatures are measured by thermoreflectance, i.e., the change in the reflectivity with temperature. This change in reflectivity is measured by changes in the reflected intensity of a probe laser beam. The probe laser beam also has a Gaussian distribution of intensity although the radius may be different than the pump beam; the $1/e^2$ radius of the probe beam is w_1. The probe beam measures a weighted average of the temperature distribution $\theta(r)$

$$\Delta\mathcal{T} = \frac{4}{w_1^2} \int_0^\infty \theta(r) \exp(-2r^2/w_1^2)\, r\, dr. \tag{8}$$

The integral over r is the Hankel transform of a Gaussian, leaving a single integral over k that must be evaluated numerically

[a)]Author to whom correspondence should be addressed; electronic mail: d-cahill@uiuc.edu

$$\Delta\mathcal{T} = 2\pi A \int_0^\infty G(k)\exp(-\pi^2 k^2(w_0^2 + w_1^2)/2)\; k\; dk. \tag{9}$$

As expected, Eq. (9) is unchanged by an exchange of the radii of the pump and probe beams. The upper limit of the integral can be set to $2/(w_0^2+w_1^2)^{1/2}$ without a significant loss of accuracy.

Before we generalize this solution to a layered structure, we examine the low and high frequency limits of Eq. (9). In our experiments, the pump and probe have the approximately the same diameter, so we set $w_0 = w_1$. In the low frequency limit, $\omega \ll D/w_0^2$,

$$\Delta\mathcal{T}_0 = \frac{A_0}{\Lambda}\int_0^\infty \exp(-\pi^2 k^2 w_0^2)\; dk, \tag{10}$$

$$= \frac{A_0}{2\sqrt{\pi} w_0 \Lambda}. \tag{11}$$

Equation (11) is particularly useful for estimating the steady-state temperature rise of the probed region of the sample. For example, with $A_0 = 2$ mW, Si thermal conductivity of $\Lambda = 142\text{W m}^{-1}\text{K}^{-1}$ and $w_0 = 8\ \mu$m, $\Delta\mathcal{T}_0 = 0.5$ K.

In the high frequency limit, $\omega \gg D/w_0^2$,

$$\Delta\mathcal{T} = \frac{A}{q\Lambda}\int_0^\infty \exp(-\pi^2 k^2 w_0^2)\; k\; dk, \tag{12}$$

$$= \frac{A}{\pi w_0^2 \sqrt{i\omega\Lambda C}}, \tag{13}$$

where C is the heat capacity per unit volume; $\sqrt{\Lambda C}$ is the thermal effusivity. Equation (13) is equivalent to the solution for one-dimensional heat flow with a uniform heat flux of $A/(\pi w_0^2)$.

III. FREQUENCY DOMAIN SOLUTION FOR THE SURFACE TEMPERATURE OF A LAYERED STRUCTURE

Equation (9) can be generalized to a layered geometry using the algorithm described recently by Feldman;[15] this algorithm has also been applied in the analysis of data[16] obtained by the 3ω method. The final result is obtained iteratively: we number the layers by $n=1$ for the layer that terminates at the surface of the solid. The iteration starts with the layer farthest from the surface; in practical applications of this method to the analysis of TDTR data, heat cannot reach the other side of this bottom layer at rates comparable to the modulation frequency; therefore, $B^+ = 0$ and $B^- = 1$ for the final layer.

$$\begin{pmatrix} B^+ \\ B^- \end{pmatrix}_n = \frac{1}{2\gamma_n}\begin{pmatrix} \exp(-u_n L_n) & 0 \\ 0 & \exp(u_n L_n) \end{pmatrix} \times \begin{pmatrix} \gamma_n + \gamma_{n+1} & \gamma_n - \gamma_{n+1} \\ \gamma_n - \gamma_{n+1} & \gamma_n + \gamma_{n+1} \end{pmatrix}\begin{pmatrix} B^+ \\ B^- \end{pmatrix}_{n+1}, \tag{14}$$

$$u_n = (4\pi^2 k^2 + q_n^2)^{1/2}, \tag{15}$$

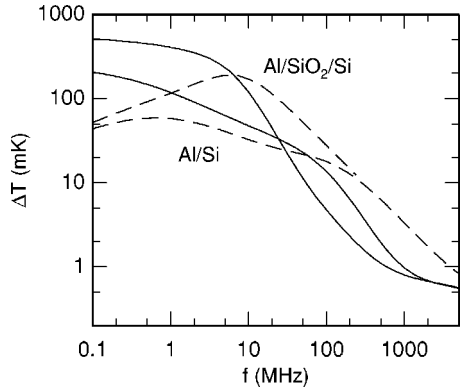

FIG. 1. Calculated frequency response of Al/Si and Al/SiO_2/Si thermal models. In both cases, the Al film thickness is 100 nm; for Al/Si, a interface thermal conductance of $G = 200\ \text{MW m}^{-2}\text{K}^{-1}$ is included in the model. For Al/SiO_2/Si, the thickness of the SiO_2 layer is 100 nm. Solid lines show the real part of $\Delta\mathcal{T}$, see Eqs. (9) and (18), and the dashed lines are the imaginary part of $\Delta\mathcal{T}$. The amplitude of the laser power absorbed by the sample is $A = 1$ mW.

$$q_n^2 = \frac{i\omega}{D_n}, \tag{16}$$

$$\gamma_n = \Lambda_n u_n. \tag{17}$$

Each layer n is described by three parameters; the thermal conductivity Λ_n, thermal diffusivity D_n, and thickness L_n. We model an interface conductance by a layer with a small thermal conductivity and small thickness.

For a layered structure, the only change in Eq. (9) is to replace $G(k)$ for the single layer [Eq. (4)] by

$$G(k) = \left(\frac{B_1^+ + B_1^-}{B_1^- - B_1^+}\right)\frac{1}{\gamma_1}. \tag{18}$$

Example calculations using the combination of Eq. (9) and Eq. (18) are shown as Fig. 1.

IV. MODELING OF DATA ACQUIRED IN TIME-DOMAIN THERMOREFLECTANCE EXPERIMENTS

We can now use the frequency-domain thermal response, Eqs. (9) and (18), to calculate the changes in reflectivity that will be measured in a TDTR experiment. Because the width of the optical pulses produced by a Ti:sapphire laser, <0.5 ps, are much shorter than the time scales of interest in the thermal model, $t > 50$ ps, we can approximate the frequency spectrum of the laser output as a series of delta functions separated in frequency by the repetition rate of the laser $1/\tau$. The pump beam is modulated by a 50% duty cycle at frequency f. This modulation reduces the magnitude of the peaks at all multiples of $1/\tau$ and produces sharp sidebands around each of these peaks at odd multiples of f; the amplitudes of the sideband at frequency f removed from the main peaks is a factor of $2/\pi$ times smaller than the amplitudes of the main peaks.

Surface temperatures are measured by the changes in reflectivity R with temperature T, i.e., the thermoreflectance dR/dT. The signal of interest is produced by the product of the temperature changes and the intensity of the probe beam; in the frequency domain this product becomes a convolution

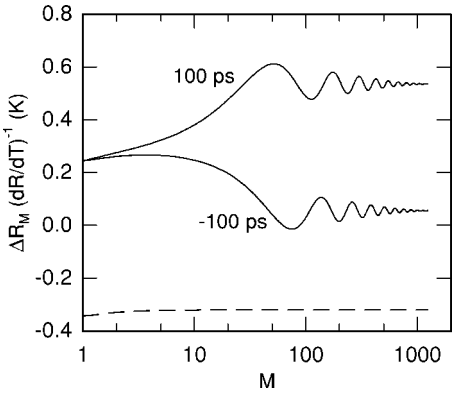

FIG. 2. Partial sums of the series used to calculate the reflectivity changes, see Eq. (19); dR/dT is the thermoreflectance of the surface. The solid lines are the real part of $\Delta R_M(t)$ evaluated for two delay times $t=100$ and $t=-100$ ps; the dashed line is the imaginary part of $\Delta R_M(t)$ and is independent of t for short delay times. The terms in the sum for the real part of $\Delta R_M(t)$ have been multiplied by a Gaussian factor of the form $\exp(-\pi(f/f_{\max})^2)$ with $f_{\max}=100$ GHz to improve the convergence of the sum. The thermal model is for $Al/SiO_2/Si$ as described in the caption to Fig. 1.

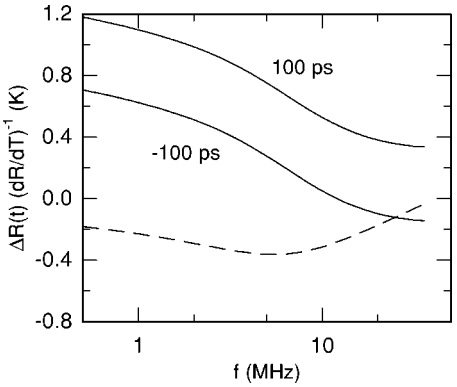

FIG. 3. Calculated dependence of the reflectivity changes at fixed delay times of 100 and −100 ps on modulation frequency f; dR/dT is the thermoreflectance of the surface. The imaginary part of the response (dashed line) is essentially constant for these two times. The thermal model is for $Al/SiO_2/Si$ as described in the caption to Fig. 1

of the frequency spectra of the thermal response and the probe beam. The time delay t shifts the relative phase of the probe frequency spectrum. The lock-in amplifier picks out the frequency components of the convolution evaluated at f and $-f$

$$\mathrm{Re}[\Delta R_M(t)] = \frac{dR}{dT}\sum_{m=-M}^{M}(\Delta\mathcal{T}(m/\tau+f) + \Delta\mathcal{T}(m/\tau-f))\exp(i2\pi mt/\tau), \tag{19}$$

$$\mathrm{Im}[\Delta R_M(t)] = -i\frac{dR}{dT}\sum_{m=-M}^{M}(\Delta\mathcal{T}(m/\tau+f) - \Delta\mathcal{T}(m/\tau-f))\exp(i2\pi mt/\tau). \tag{20}$$

The power absorbed by the sample from the pump beam at frequency f, A_f, is related to the average power absorbed from the pump beam A_0 by $A_f=2A_0/\pi$.

We plot the partial sums $\Delta R_M(t)$ as Fig. 2 to illustrate which frequency components of $\Delta\mathcal{T}$ contribute to the real and imaginary parts of the reflectivity signal. The imaginary part $\Delta R_M(t)$ converges rapidly after only a few terms. The real part of $\Delta R_M(t)$ converges slowly: to speed up the convergence, we multiply each term by a Gaussian factor $\exp(-\pi(f/f_{\max})^2)$ where $f_{\max}$ is the maximum frequency that is considered in the calculation. We find smooth and accurate reproduction of the experimental data by choosing $f_{\max}=10/t_{\min}$ where $t_{\min}$ is the absolute value of the minimum delay time that will be considered in the analysis.

Convergence of the real part of $\Delta R_M(t)$ is also facilitated by replacing the top 10 nm of the Al metal film at the surface of the sample by a 1 nm layer that has ten times the true heat capacity and ten times the true thermal conductivity of the Al film. This mimics the adsorption of laser energy within the thickness of the optical absorption depth without changing the heat capacity per unit area of the Al film or the lateral thermal diffusivity of the Al film.

In our implementation of TDTR, the arrival time of the pump beam is advanced rather than the more typical case of increasing the delay time of the probe beam. This procedure introduces an additional phase shift

$$\Delta R(t) = \Delta R_M(t)\exp(i2\pi ft) \tag{21}$$

with the limit of the sum set to $M=10\tau/t$.

The dependence of $\Delta R(t)$ on the modulation frequency f is illustrated by Fig. 3 for fixed delay times of $t=\pm 100$ ps. In principle, the optimal choice of f will depend on the system under study. In practice, we prefer $f\approx 1/(8\tau)\approx 10$ MHz where the real part of $\Delta R(t)$ is minimized at negative delay times. We have occasionally used lower values of f to increase the penetration depth of the thermal waves[10] but a relatively high modulation frequency is desirable for high spatial resolution[11] and to minimize the influence of uncertainties in the diameter of the laser beam.

Typically, a rf lock-in amplifier incorporates a square-wave mixer and therefore the input signal from the photodetector must be filtered to remove the odd harmonics of f that are present in the intensity of the reflected probe. In our apparatus, a tunable inductor is placed in series between the output of a reversed biased *p-i-n* Si photodiode and the 50 Ω input of the rf lock-in amplifier.[17] The inductance and the modulation frequency f are adjusted to maximize the response at f; the quality factor of the resonant circuit is $Q\approx 10$. The rms voltage measured by the lock-in amplifier at the modulation frequency f, $V_f(t)$, is related to the changes in reflectivity by

$$\frac{V_f(t)}{V_0} = \frac{Q}{\sqrt{2}}\frac{\Delta R(t)}{R}, \tag{22}$$

where V_0 is the average voltage output of the detector and R is the reflectivity of the sample. The real and imaginary parts of $V_f(t)$ are given by the in-phase and out-of-phase signals of the lock-in amplifier, respectively. We use the fact that the imaginary part of $V_f(t)$ is constant as the delay time crosses $t=0$ to correct for small errors in the phase ε of the reference channel of the lock-in amplifier by multiplying $V_f(t)$ by a small phase factor of the form $(1-i\varepsilon)$.

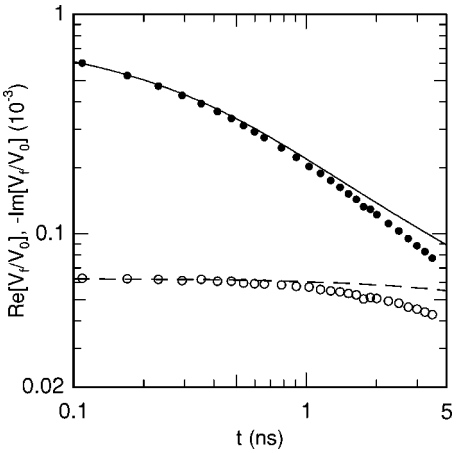

FIG. 4. Dependence on delay time t at fixed modulation frequency of $f=9.8$ MHz for a TiN/MgO(001) epitaxial layer. Measured data are shown as filled circles [in-phase or real part of $V_f(t)$] and open circles [out-of-phase or imaginary part of $V_f(t)$]. The solid and dashed lines are the real and imaginary parts of the model calculation, respectively, see Eq. (22).

We compare an example of a full calculation of $V_f(t)/V_0$ to measured data in Fig. 4. The unknown layer parameters in the fit—the thickness of the TiN layer (56 nm) and the thermal conductance of the TiN/MgO interface ($650\ \mathrm{MW\,m^{-2}\,K^{-1}}$)—were measured in a fit to the ratio V_{in}/V_{out} as described in Ref. 8. The thermoreflectance was also adjusted to improve the fit shown in Fig. 4; we find $dR/dT=1.8\times10^{-4}\ \mathrm{K^{-1}}$. This value for dR/dT is in good agreement with measurements by ellipsometry, $1.6\times10^{-4}\ \mathrm{K^{-1}}$.

The deviation of the data from the fits at large delay times, $t>2$ ns is caused by the changes in the radius of the pump beam w_0 with changes in the length of the optical path of the pump beam; i.e., the model calculation assumes that w_0 is constant but in reality w_0 varies with delay time t. We have previously discussed how our approach of analyzing the ratio $V_{\mathrm{in}}/V_{\mathrm{out}}$ minimizes these errors;[6,8] the optical design of Capinski and Maris[3] provides another method for improving the accuracy of TDTR measurements at large delay times.

This work was supported by NSF Grant No. CTS-0319235. Data were acquired using the equipment in the Laser Facility of the Frederick Seitz Materials Research Laboratory (MRL) at the University of Illinois at Urbana-Champaign.

[1] D. A. Young, C. Thomsen, H. T. Grahn, H. J. Maris, and J. Tauc, in *Phonon Scattering in Condensed Matter*, edited by A. C. Anderson and J. P. Wolfe (Springer, Berlin, 1986), p. 49.
[2] C. A. Paddock and G. L. Eesley, J. Appl. Phys. **60**, 285 (1986).
[3] W. S. Capinski and H. J. Maris, Rev. Sci. Instrum. **67**, 2720 (1996).
[4] B. Bonello, B. Perrin, and C. Rossignol, J. Appl. Phys. **83**, 3081 (1998).
[5] N. Taketoshi, T. Baba, E. Schaub, and A. Ono, Rev. Sci. Instrum. **74**, 5226 (2003).
[6] D. G. Cahill, K. E. Goodson, and A. Majumdar, J. Heat Transfer **124**, 223 (2002).
[7] D. G. Cahill, W. K. Ford, K. E. Goodson, G. D. Mahan, A. Majumdar, H. J. Maris, R. Merlin, and S. R. Phillpot, J. Appl. Phys. **93**, 793 (2003).
[8] R. M. Costescu, M. A. Wall, and D. G. Cahill, Phys. Rev. B **67**, 054302 (2003).
[9] R. M. Costescu, D. G. Cahill, F. H. Fabreguette, Z. A. Sechrist, and S. M. George, Science **303**, 989 (2004).
[10] S. Huxtable, D. G. Cahill, and L. M. Phinney, J. Appl. Phys. **95**, 2102 (2004).
[11] S. Huxtable, D. G. Cahill, V. Fauconnier, J. O. White, and J.-C. Zhao, Nat. Mater. **3**, 298 (2004).
[12] H. S. Carslaw and J. C. Jaeger, *Conduction of Heat in Solids* (Oxford University Press, New York, 1959), p. 263.
[13] R. N. Bracewell, *The Fourier Transform and its Applications* (McGraw–Hill, New York, 2000), Chap. 13, pp. 335–339.
[14] Y. Ohsone, G. Wu, J. Dryden, F. Zok, and A. Majumdar, J. Heat Transfer **121**, 954 (1999).
[15] A. Feldman, High Temp. - High Press. **31**, 293 (1999).
[16] J. H. Kim, A. Feldman, and D. Novotny, J. Appl. Phys. **86**, 3959 (1999).
[17] K. E. O'Hara, X.-Y. Hu, and D. G. Cahill, J. Appl. Phys. **90**, 4852 (2001).